Beam-propagation analysis of loss in bent optical waveguides and fibers

J. Saijonmaa

Department of Electrical Engineering, Communications Laboratory, Helsinki University of Technology, 02150 Espoo 15, Finland

D. Yevick

Institute of Optical Research, S-100 44 Stockholm, Sweden

Received February 26, 1983; revised manuscript received July 7, 1983

We demonstrate that the beam-propagation method can be used to calculate accurately both the pure bending loss and the transition loss of bent single-mode optical waveguides and fibers. Our results allow us to establish the accuracy of several commonly used theories of bending loss and to investigate the degree to which theories of step-index monomode fiber losses can be used to predict the losses of graded-index monomode fibers.

1. INTRODUCTION

A single-mode fiber in an optical fiber system generally contains both large-radii bends arising from the layout geometry of the optical fiber link and microbends generated principally in jacketing and cabling processes. Bending loss that is highly dependent on fiber parameters, such as the radius of curvature and the refractive-index difference, can also be exploited in sensor applications if the dependence of the loss on the curvature radius is accurately known. Consequently, much theoretical attention was devoted in the past to the characterization of the loss of bent single-mode fibers. Here two types of loss have been distinguished: the pure bending loss, which is the loss approached asymptotically in a fiber with a constant radius of curvature,[1] and the transition loss, which occurs at the beginning of a bend and is associated with the rate of change of the curvature radius.[2–4] The latter mechanism dominates in so-called strong bends, that is, bends with small curvature radii, whereas both mechanisms are usually of importance in microbends.[5]

Previous studies of the transition loss were based on couple-mode and perturbation theory analyses of the power in the radiation modes.[1,5] These theories, however, have the disadvantage that they assume either that all power coupled into the radiation modes immediately escapes from the core region or that none of the power escapes.[1] The pure bending loss, on the other hand, has been analyzed rigorously for step-index fibers, and concise expressions for this loss have been derived by several authors.[6,7] These formulas were modified later to incorporate graded-index single-mode fibers[8] and applied to alpha profiles using a power-series solution of the wave equation. The accuracy to which the bending loss of a graded-index fiber can be calculated by using its equivalent step-index (ESI) profile is an associated problem of great theoretical interest, as the bending loss is still a parameter for which the accuracy of the ESI methods has not been established. Since different criteria in determining the ESI profile yield slightly different step-index parameters and since the bending loss is a strongly sensitive function of these parameters, the determination of the ESI criteria that most accurately predict the bending loss of graded-index monomode fibers is of great importance.

In this paper we investigate these and related problems by means of the beam-propagation method (BPM), which takes into account the actual loss of power coupled to the radiating modes and can be applied to almost arbitrary single-mode refractive-index profiles. By using this method we are able to evaluate the accuracy of different theories of transition loss and of different ESI criteria for the pure bending loss of graded-index single-mode profiles.

Although bending losses of rectangular integrated-optics waveguides were studied recently by Baets and Lagasse,[9] these authors employ an approximate effective-index method to reduce the dimensionality of their problem, thus eliminating many of the difficulties encountered in our three-dimensional fiber-optics computations.

2. NUMERICAL METHOD

The BPM is a simple and accurate numerical procedure for describing the propagation of an arbitrary incoming optical field through a given optical system. The method can be based on either the full scalar-wave equation for the electric field, as discussed in Ref. 10, or on the Fresnel equation that is valid for paraxial field propagation. In this paper we adopt the Fresnel equation formalism, which yields the following relation between the electric fields at adjacent planes perpendicular to the optical axis and separated by a distance dz:

$$E(x,y,z+dz) = \exp\left(-\frac{i dz}{4n_0 k}\nabla_\perp{}^2\right) \times \exp\left\{-\frac{in_0 k}{2}\int_z^{z+dz}[n(x,y,z')^2/n_0{}^2 - 1]dz'\right\} \times \exp\left(-\frac{i dz}{4n_0 k}\nabla_\perp{}^2\right) E(x,y,z)\exp(-ikn_0 dz) + O(dz)^3. \quad (1)$$

Here n_0 denotes the cladding refractive index, $k = \omega/c$ is the

0030-3941/83/121785-07$01.00

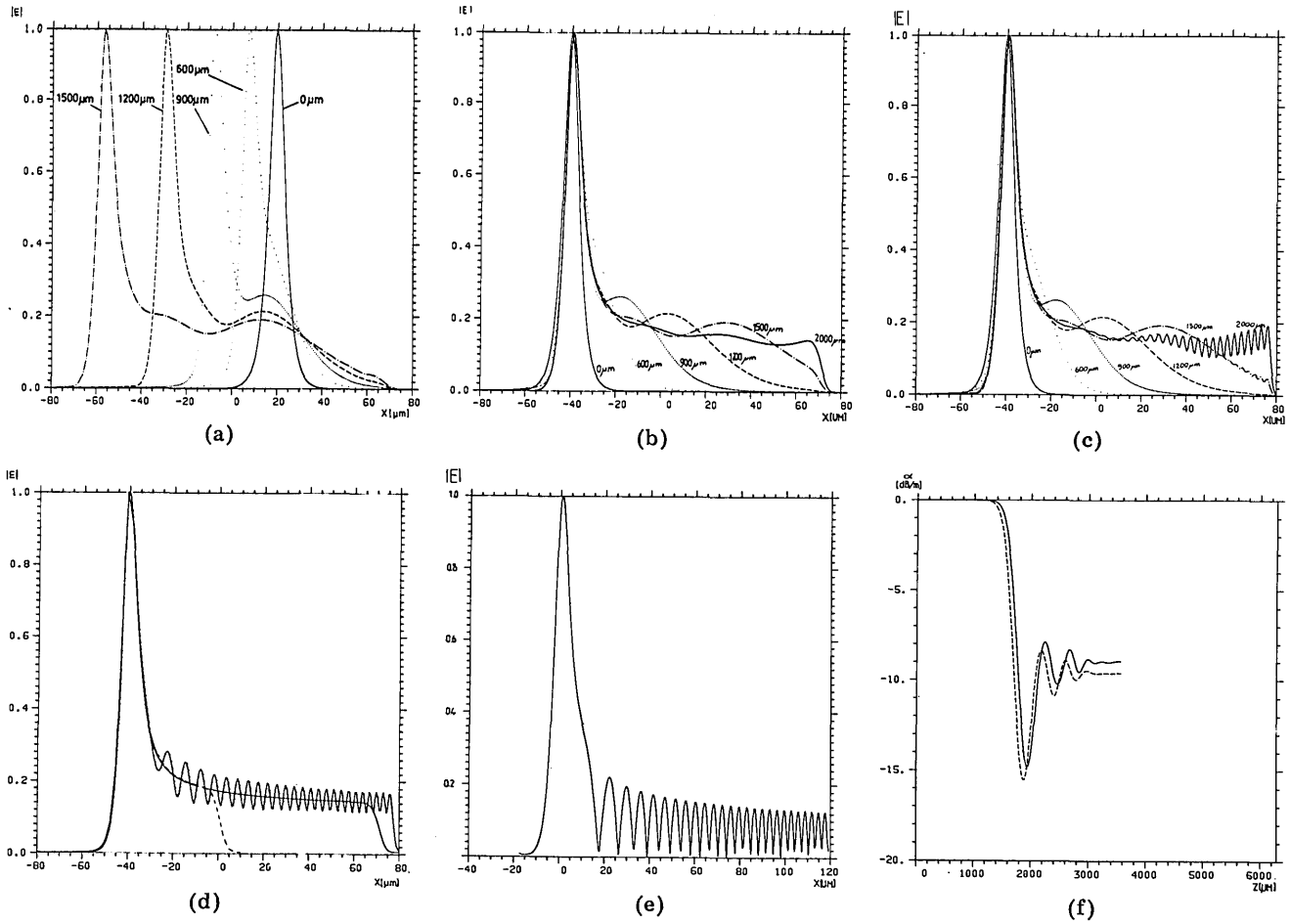

Fig. 1. (a) Electric field distributions in a bent two-dimensional cosh profile at axial distances 0 to 1500 μm from the start of the bend in a fixed coordinate system, computed with a 160-μm-wide window and 256 grid points, $V = 1.4$, $a = 3$ μm, and $R = 1.5$ cm. (b) Electric field distributions as in (a) in a coordinate system moving with the fiber axis [Eq. (5)] at axial distances 0 to 2000 μm from the start of the bend; 20-μm-thick absorbers are used at window distance 60–80 μm from the origin of the window (middle point). (c) Same as (b) but with 3-μm-thick absorbers (at 77–80 μm from the origin). (d) Asymptotic bent waveguide field distributions ($z = 3000$ μm) of (b) and (c) computed with thick (solid line) and thin (dotted solid line) absorbers. The dashed-line field distribution corresponds to a thick absorber placed 30–50 μm from the waveguide axis, computed with 32 grid points. (e) Asymptotic field distribution of (d) computed by direct integration of the wave equation in a bent waveguide. (f) Differential power loss from the computational window as a function of propagation distance from the start of the bend expressed in decibels per meter for the waveguide computed with the 20-μm absorber (dashed line) and the 3-μm absorber (solid line) of (d).

light wave number in vacuum, and $\nabla_\perp$ is the Laplacian operator in the transverse (x, y) plane. The electric field in Eq. (1) is Fourier transformed before multiplication by each exponential operator containing $\nabla_\perp$ (d/dx and d/dy are then replaced by k_x and k_y), and the result is then inverse Fourier transformed before multiplication by the subsequent exponential operator containing $n(x, y, z)$. Because of the rapidity of the fast-Fourier-transformation technique, repeating this procedure a prescribed number of times allows us to evaluate relatively simply the electric field at a given distance from the input face of the optical element. We can check our results either by a direct comparison with analytical results, as in this paper, or by repeating the calculation using a different step length dz.

Equation (1) can also be used to determine the propagation constants and excitation coefficients of the modes comprising a given incoming excitation.[11] These are calculated by evaluating the correlation function:

$$C(z) = \iint \varepsilon(x, y, 0)^* \varepsilon(x, y, z)\mathrm{d}x\mathrm{d}y,$$

$$\varepsilon(x, y, z) = \exp(-ikn_0 z)E(x, y, z), \qquad (2)$$

after each step as the electric field is propagated a distance Mdz through the waveguide or the fiber length. Multiplying $C(z)$ by a suitable window function and Fourier transforming, we obtain a curve marked by sharp peaks centered at the positions of the bound-state propagation constants. The exact positions of the peaks must be determined by a suitable curve-fitting procedure.[11]

A physical interpretation of Eq. (1) is that we have replaced the actual continuous refractive-index distribution of the optical element with a series of infinitesimally thin lenses separated by a distance dz in a homogeneous medium with the refractive index of the cladding. The phase change imparted to the electric field by each of the infinitesimally thin elements is then the phase change that would be imparted continuously to the field in the true profile in the absence of diffraction effects.

A problem in the beam-propagation technique, which is of primary concern in optical loss calculations, is that the electric field that propagates to the edge of the computational window in the transverse (x, y) plane will, in succeeding steps, be folded back to the opposite edge of the window, causing

high-frequency numerical instabilities. In order to avoid this problem, we must absorb the field at the edge of the window, for example, by setting the electric field at the first and last few window grid points to zero or by inserting a large negative imaginary component in the refractive index at these points, as was first suggested and analyzed in Ref. 10. If we follow this procedure in a configuration in which the electric field at the absorber boundary reaches large values, however, we rapidly find that a large-amplitude high-frequency ripple is implanted on the electric field inside the window, as in Fig. 1(c). The origin of the ripple is, of course, the diffraction phenomenon associated with the sharp falloff of the field. Therefore the absorber must be constructed to ensure that the electric field be absorbed gradually near the window boundaries. As we show in Section 3, a suitable absorber in two-dimensional calculations is obtained if the electric field is multiplied by the following function:

$$\text{absorb}(x) = \begin{cases} 1, & |x| < |x_a|, \\ 1/2\{1 + \cos^{\gamma}[\pi(x - x_b)/(x_a - x_b)]\}, & |x_a| < |x| < |x_b|, \\ 0, & |x_b| < |x| < |x_R|, \end{cases} \tag{3}$$

where x_R is the coordinate of the grid boundary, x_a denotes the inner edge of the absorber, and x_b is the outer edge. The parameters γ, x_a, and x_b are chosen empirically for each problem configuration and step length to ensure that the field is absorbed gradually over a sufficiently wide region $|x_a| < |x| < |x_b|$. The distance between x_b and x_R is adjusted similarly according to the step size and the shape of the Fourier spectrum of the electric field at large wave numbers to ensure that no interference effects will occur as a result of folding back of the electric field at the edges of the computational window. x_a must be choosen far enough from the axis so that in a lossless straight fiber the absorber does not perceptably affect the guided field distributions. The transverse y direction must be treated analogously.

3. RESULTS

Although most of this section is devoted to comparisons of the results of various theoretical methods with those of the BPM, first we establish the applicability of the BPM to single-mode structures and illustrate the effects of various absorber profiles. Our first demonstration of the accuracy of the beam-propagation technique regards the computation of the propagation constants of the lowest-order modes of unperturbed parabolic-index fibers with V values ranging from 1.5 to 5. A comparison of our values with the analytical results of Ref. 12 is shown in Fig. 2. The discrepancy between the two sets of

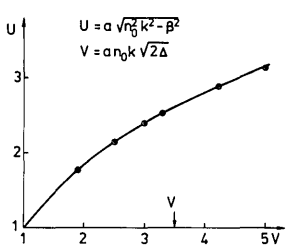

Fig. 2. Comparison of the normalized propagation constant of a parabolic single-mode fiber, computed with the BPM, with that computed by Gambling.[4]

results is less than 1%, which indicates that the BPM correctly predicts the overall properties of the propagating field in a single-mode fiber. A 64 × 64 point computational window has been employed, and the electric field has been evaluated at 128 axial points over a propagation distance of 2500 μm. The accuracy of the BPM constants could be further increased by increasing the propagation length and the number of sample points. The propagation constant of the fundamental mode was independent of the absorber structure as long as we excited the fiber with an electric field distribution close to that of the fiber's guided mode. We note parenthetically that, once the propagation constants are determined, the wave functions can be evaluated by using the procedure described in Ref. 11. The convergence of this procedure, however, is slow and requires the use of proper absorbers, chosen according to the criteria stated in Section 2, at the window boundaries. Therefore the wave functions employed in this paper have been evaluated either analytically or by applying the shooting method and direct integration of the scalar-wave equation.

The new and crucial feature of our BPM calculations is the use of the absorber structure described in Section 2. We therefore discuss first the dependence of the electric field on the absorber structure in a two-dimensional waveguide, with an index profile given by

$$n(x)^2 = n_{cl}^2 + 2\Delta n_{cl}^2/\cosh^2(x/a), \tag{4}$$

where Δ is the refractive-index difference and a is the effective core radius. The eigenfunctions of this profile are easily computed analytically and are found, for example, in Ref. 13.

We can approximately model a bent waveguide with this profile either by simply shifting the center of the profile in the transverse direction as the field is propagated, thus simulating the bend, or more exactly by considering the equivalent problem of a straight fiber with an index profile given as the sum of Eq. (4) and a correction term[5]:

$$n_{eq}^2 = n^2 + 2xn_{cl}^2/R, \tag{5}$$

where R is the bend radius and x is the coordinate along the radius of curvature. The disadvantage of the former method is that only the beginning of the bend can be analyzed because the rotation of the index profile in the direction of the optical axis, which increases linearly with the bend length, is not accounted for. Also, the absorber, which is here given by Eq. (3) with $|x_a - x_b| = 18$ μm and $\beta = 2$, may affect the electric field somewhat differently, depending on which of the above two methods is employed. A comparison of the electric fields computed with each of the two methods can therefore establish the validity of Eq. (5) and demonstrate that the thick absorber has little effect on the electric field inside the window. Accordingly, the electric fields at axial distances of 0, 600, 900, 1200, 1500, and 2000 μm from the start of the bend, computed with a 256-point transverse grid according to the method of shifting the index profile and according to the equivalent straight waveguide method, are given in Figs. 1(a) and 1(b), respectively. The waveguide profile is given by Eq. (4) with $a = 3$ μm and $V = 1.4$ at the second-order mode cutoff of the straight fiber, while the bending radius $R = 1.5$ cm. The waveguide is excited with the straight fiber fundamental mode so that no refracted modes are present at the start of the

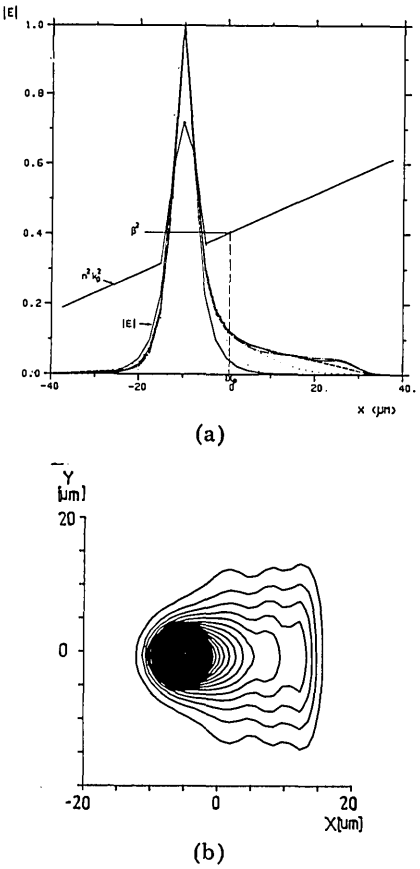

Fig. 3. (a) Field distributions of a bent (three-dimensional) fiber computed at axial distances from 0 to 2000 μm from the start of the bend using a 20-μm-wide absorber and a 32 × 32 computational window. Also shown are the effective refractive-index distribution (n^2k^2) along with the propagation constant β and turning point x_p. The fiber is a parabolic single-mode fiber with $V = 2$, $a = 3$ μm, and $R = 2.5$ cm. (b) Asymptotic field distribution of (a) shown as a contour plot in the transverse fiber plane.

bend. In all the calculations in this paper, the step length $dz = 10$ μm and wavelength $\lambda = 1$ μm, whereas the field distributions are always normalized so that their maximum value is unity. As Figs. 1(a) and 1(b) agree well, we conclude that a thick absorber has little effect on the electric fields inside the window, provided, of course, that the inner absorber edge lies outside the classical turning point of the leaky fundamental mode of the bent waveguide, point x_p in Fig. 3(a). However, decreasing the absorber width to 3 μm destroys the validity of our results, as is shown in Figure 1(c). Clearly, a high-frequency diffraction pattern rapidly develops once the electric field, escaping from the bent fiber core, reaches the window edge. The wavelength of the ripple of the diffraction pattern is a function of the light frequency and remains unchanged if the absorber thickness is varied slightly. However, the average shape of the field is independent of the absorber structure. This can be seen best from Fig. 1(d), which shows the steady-state distribution of the electric field, reached after a propagation distance of 3 mm. The three curves in the figure have been calculated with a thick absorber with a 160-μm-wide window and 256 grid points (solid line), a thin absorber with the same window and grid-point structure (dotted–dashed line), and a thick absorber with a 80-μm window and 32 grid points (dashed line). We notice also from the figure that the field distribution is independent of the absorber position. Consequently we are able to decrease the number of points in our computational grid, and, in fact, satisfactory results are obtained for the field amplitudes when only six grid points fall within the effective core region, which here is 6 μm thick. This observation allows us to perform calculations in three dimensions easily.

Turning next to the influence of the absorber structure on the differential power loss, which is calculated by evaluating the difference in the integrated optical power in the 160-μm computational window between two adjacent axial propagation steps, and expressing the result in decibels per meter, we find the results given by the dashed and solid lines in Figure 1(f) for the thick and thin absorbers, respectively. Although the loss of the thin-absorber curve is about 5% less than that of the thick-absorber curve, indicating that the high-frequency ripple in the field diffracted by the thin absorber carries a certain amount of diffracted energy, the form of the results is remarkably similar. The slight axial displacement of the curves is caused, of course, by the different location of the inner edge of the absorbers with respect to the waveguide center. Repeating the calculations with a 32-point 80-μm-guide computational grid also yielded fairly accurate results for the differential loss.

Having discussed the structure of our program in some detail, we now compare our two-dimensional power loss and electric field distributions with the predictions of analytic theories in order better to understand and evaluate the features of our results. As we noted earlier, the bending loss can be expressed as the sum of the pure bending loss, which corresponds to the loss approached asymptotically at large axial distances in the curves of Fig. 1(f), and the transition loss, which is the loss associated with the rapid fluctuation in the figures at small axial distances. The pure bending loss is the loss intrinsic to the lowest-order mode of the bent waveguide, whereas the transition loss is associated with the power coupled to higher-order radiating modes. We now consider each of the two types of loss separately.

A simple method for examining the origin of the pure bending loss is to compare the electric field amplitude in the pure-bending-loss region, Fig. 1(d), with the electric field amplitude obtained by direct numerical integration of the scalar-wave equation in the equivalent straight waveguide profile, Fig. 1(e). In comparing Figs. 1(b) and 1(e), however, we must observe that the actual radiating electric field is built up over a finite axial distance and contains a range of β values in the radiating region as a result of tunneling phenomena. Therefore the BPM results do not display the rapid oscillation of the wave function generated by direct numerical integration in the region outside the classical turning point.

We next turn our consideration from the pure-bending-loss region to the transition-loss region. Here we observe from Figs. 1(a) and 1(b) that the electric field rapidly develops subsidary maxima. The first of these maxima is seen most clearly in the curve for the electric field after a propagation distance of $z = 1200$ μm, whereas two other maxima can be resolved in the $z = 2000$-μm curve. Although the position of these maxima in a fixed coordinate system is actually effectively constant, as can be seen from Fig. 1(a), replacing the bent-fiber profile with an equivalent straight profile, Eq. (5), is equivalent to transforming to a coordinate system that is rotated and displaced continuously to ensure that the origin

coincides with the fiber center and the direction of the z axis with the tangent to the fiber axis. Since the velocity of this coordinate system in a fixed reference frame will be constantly increasing, the first subsidiary refracted power maximum is absorbed over a larger propagation length than the following maxima. This is clearly seen in the form of the power-loss curves [Fig. 1(f)] as the fluctuation in the power loss increases somewhat in frequency at larger axial distances. Although no previous calculations have addressed the problem of describing the actual electric field structure in the transition region, such effects can be studied in perturbation theory by calculating the coupling between the fundamental mode and an arbitrary radiation mode of the straight unperturbed fiber induced by the bend. If we then associate the total power in all the radiation modes with the transition loss, we arrive at a simplified model of the transition effects. Accordingly, we have therefore to evaluate numerically the coupling integral[1]:

$$K(\beta) = \frac{\omega\varepsilon_0}{4i}\int_{-\infty}^{+\infty} \delta n^2 E_0(\beta_0) E_\beta(\beta)^* \mathrm{d}x, \tag{6}$$

where δn^2 is the perturbation term in the index profile [Eq. (5)], E_0 is the fundamental mode field and β_0 is its propagation constant, and E_β is the radiation mode field with propagation constant β. The radiated power at axial distance z is then approximated by the integral

$$P(z) = \int_0^{kn_{cl}} K(\beta)^2 \left| (1/z^{1/2}) \int_0^z \exp[-i(\beta-\beta_0)z]\mathrm{d}z \right|^2 \mathrm{d}\beta. \tag{7}$$

Here we neglect backward-traveling waves. The term $P(z)$ computed by this procedure for a waveguide profile, given by $a = 3\ \mu$m, $V = 1.4$, and $R = 1.5$ cm, is shown in Fig. 4 (solid line). The dashed line in this figure incorporates a simple approximation, which is due to Marcuse,[4] who modeled the fundamental-mode field distribution by a Gaussian function and the radiating mode by a sinusoidal function. As the fundamental mode of the cosh profile is somewhat wider than the Gaussian-function approximation predicts, the overlap integrals in Eq. (6) are severely underestimated in Marcuse's method. If we now define a normalized oscillation frequency from our BPM results by dividing the number of fluctuations on the radiated power curve after a given propagation length with the propagation length, we find that the resultant value agrees quite well with the frequency of the perturbation theory curves. The amplitude of the first transition-loss oscillation

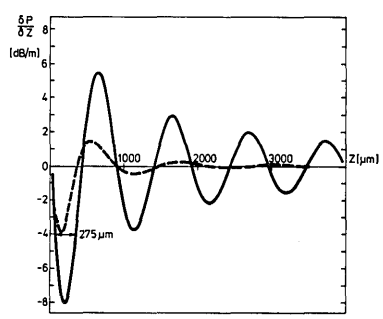

Fig. 4. Differential power coupled into higher-order radiated modes in the waveguide of Fig. 1(a), computed with perturbation theory. The dashed curve corresponds to approximating the fundamental and radiated modal fields by simple analytical functions (see text).

computed with the BPM relative to the steady-state power-loss level is also in good agreement with perturbation theory. However, the amplitudes of the subsequent maxima are not correctly predicted by perturbation theory. This discrepancy arises principally because Eqs. (6) and (7) neglect the propagation of the radiating modes away from the waveguide core and the subsequent development of a steady-state electric field distribution.

Having established the validity of our numerical procedure by various qualitative and quantitative comparisons in two dimensions, we are prepared to make quantitative predictions of the bending loss of graded-index single-mode fibers. We accordingly study the bending loss as a function of curvature radius of two single-mode parabolic graded-index fibers. The first of these has a V value of 2, which is 59% of the cutoff V value, and a core radius of $a = 3\ \mu$m. The second, more typical profile has a V value of 3, which is 89% of the cutoff V value, and a core radius of $a = 4.5\ \mu$m. Of these two fibers, we naturally expect that the latter will display a stronger dependence of the bending loss on the curvature radius. In accordance with our two-dimensional results, we are able to perform our calculation with a 32×32 point grid. The excitation field is the guided mode of the straight fiber, which we determine through a numerical integration program. Because our computations are performed to seven-digit accuracy, loss levels less than 0.1 dB/m fall below the numerical resolution of our program.

Following the pattern of our two-dimensional discussion, we first display in Fig. 3(a) the electric field distributions along the radius of curvature at various axial distances from 0 to 3000 μm from the start of the bend. The fiber parameters in the figure are $V = 2$, $a = 3\ \mu$m, and $R = 2$ cm. In the same figure we show the fiber's refractive-index profile as resolved by the program together with the propagation constant of the unperturbed fiber's fundamental mode. Clearly, the absorber is located well outside the classical turning point (x_p) of the leaky fundamental mode. A contour plot of the steady-state field distribution in the transverse plane is given in Fig. 3(b). The influence of the absorber is clearly evident in the slow decay of the electric field to zero at the right-hand side of the computational window. Finally, the power-loss curves of the fiber considered for radii of curvature from 1 to 5 cm are shown in Fig. 5(a). Here we see that doubling the bending radius decreases the bending loss by 32 dB, whereas the transient loss decreases by only a factor of about 5. Since the acceleration of our computational window with respect to a fixed reference frame depends on the value chosen for the bending radius, the minima and maxima of the transient losses shift to the right at larger bending radii. However, the overall structure of the transient loss is quite independent of bending radius, in agreement with perturbation theory.

Considering next the $V = 3$ fiber, we discover from Fig. 5(b) that doubling the bending radius now induces a 64-dB decrease in the bending loss, whereas the form of the transition loss is again relatively constant. Our results for the magnitude of the transition loss as a function of curvature radius can be readily compared with the simplified perturbation-theory model. This model, discused in Refs. 1 and 2, estimates the transition loss from the overlap of two Gaussian functions displaced a distance equivalent to the shift of the maximum of the guided mode of the bent fiber from that of the guided mode of the straight fiber. The transition loss computed from

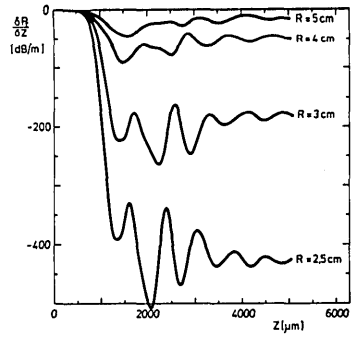

(a)

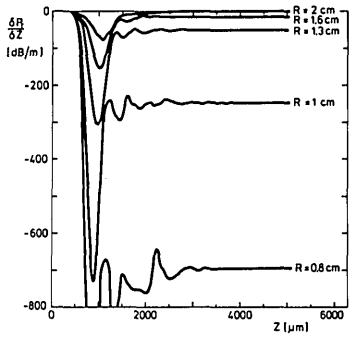

(b)

Fig. 5. Differential bending loss as a function of propagation distance in a parabolic fiber with (a) $V = 2$ and $a = 3$ μm and (b) $V = 3$ and $a = 4.5$ μm with various bending radii R from 0.8 to 5 cm.

Table 1. Transition Loss in a Bent Parabolic Single-Mode Fiber

R (cm)	α (dB) Perturbation $V = 2$	α (dB) Perturbation $V = 3$	α (dB) BPM $V = 2$	α (dB) BPM $V = 3$
0.8		0.425		0.210
1.0	0.118	0.267	0.322	0.144
1.3		0.156		0.100
1.5	0.052		0.148	
1.6		0.102		0.087
2.0	0.029	0.065	0.061	0.040
2.5	0.019	0.042	0.030	
3.0	0.013	0.029		0.020
4.0	0.007	0.016		0.013
5.0	0.005	0.010		0.009

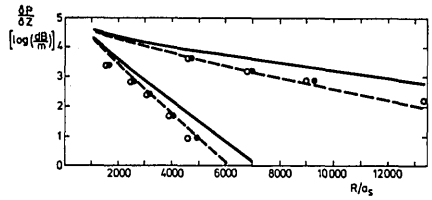

Fig. 6. Comparison of the BPM pure bending loss (circles) in the two parabolic fibers of Fig. 5 with that of ESI profiles, computed by the methods of Matsumara (solid lines) and Brinkmeyer (dashed lines).

this model is given by

$$\alpha = (R/a)^{-2}\frac{V^4}{32\Delta^2}(0.65 + 1.62V^{-1.5} + 2.88V^{-6})^6. \quad (8)$$

A comparison of the transition loss computed from Eq. (8) with our BPM result is given in Table 1. We find that, in the case $V = 3$, perturbation theory is in good agreement with the BPM result, as expected, whereas, for small bending radii, perturbation theory predicts too large a bending loss. For the $V = 2$ fiber, in which the transition takes place more slowly, the results deviate by a factor of 2–3, indicating that the approximation of instantaneous radiating-power loss in the perturbation model fails for such small V values.

We have also attempted to compare our pure-bending-loss results with existing theories. Unfortunately, because no analytic expressions exist for the pure bending loss of gradient-index single-mode fibers, we employ results for ESI fiber losses.[6,7] However, the parameters of the ESI profile associated with a given graded-index fiber are determined differently by different authors.[14–16] In Fig. 6 we compare our BPM pure-bending-loss results with the losses of the ESI fibers computed with the methods of Brinkmeyer[14] and Matsumura.[15] The theoretical results are highly sensitive to the values of the propagation constant of the straight graded-index fiber profile, which has therefore been computed analytically. The Brinkmeyer results in Fig. 6 are shown as the dashed lines and should be compared with the BPM results for the loss as a function of the scaled radius of curvature R/a, given by open circles in the figure. As the Matsumara results, given by the solid lines in the figure, imply a slightly different scaling of the radius of curvature, i.e., the effective core radius a_s, the BPM results must be rescaled to the points marked by solid circles in the figure in order to effect an exact comparison. Our results clearly show that the Brinkmeyer ESI results are in good agreement with those of BPM, whereas the Matsumara approach predicts losses that are too large by a factor of about 2. It should be noted, however, that the ESI losses are highly sensitive functions of the ESI parameters a_s and V_s.

4. CONCLUSION

We have shown that, if the electric field is properly absorbed at the edges of the computational window, the BPM can be employed to calculate the bending losses of single-mode waveguides and fibers. Our results for transition losses, although not of a form that facilitates comparisons with other theoretical approaches, indicate that perturbation theories give a somewhat misleading picture of the transition loss, especially in fibers with small V values and small-radius bends. Our pure-bending-loss results, however, show that the ESI method of Brinkmeyer can be used accurately to predict the bending loss of a parabolic-index fiber. Consequently, we can conclude that previous analytical methods can be successfully used to estimate the losses of long lengths of bent monomode fibers but not of sinusoidally bent fibers with small curvature radii.

Although the BPM can be relatively simply employed in bending-loss calculations, several drawbacks that may influence future applications of the method should be noted. First, large-radii bends with small losses cannot be analyzed by the BPM because of the limited numerical accuracy of the procedure. Profiles with rapidly varying components are also difficult to analyze if extensive computation times are to be avoided. Finally, although an absorber structure and step length that ensure that the electric field and scattered power behave smoothly can generally be determined without much trouble, diffraction effects from the electric field at the ab-

sorber boundary will always contaminate the electric field distribution to some extent further inside the computational window. Therefore it is often advisable to compare results obtained with two absorber thicknesses in order to determine the degree of accuracy of a given result.

REFERENCES

1. W. A. Gambling, H. Matsumura, and C. M. Ragdale, "Curvature and microbending losses in single-mode optical fibers," Opt. Quantum Electron. **11,** 43–58 (1979).
2. W. A. Gambling, H. Matsumura, and C. M. Ragdale, "Field deformation in curved single-mode fibers," Electron. Lett. **14,** 130–132 (1978).
3. R. A. Sammut, "Discrete radiation from curved single-mode fibers," Electron. Lett. **13,** 418–419 (1977).
4. D. Marcuse, "Radiation losses of parabolic-index slabs and fibers with bent axes," Appl. Opt. **17,** 755–768 (1978).
5. K. Petermann, "Microbending loss in monomode fibers," Electron. Lett. **12,** 107–109 (1976).
6. D. Marcuse, "Curvature loss formula for optical fibers," J. Opt. Soc. Am. **66,** 216–220 (1976).
7. L. Lewin, "Radiation from curved dielectric slabs and fibers," IEEE Trans. Microwave Theory Tech. **MTT-22,** 718–727 (1974).
8. W. A. Gambling and H. Matsumura, "Propagation in radially-inhomogeneous single-mode fibre," Opt. Quantum Electron. **10,** 31 (1978).
9. R. Baets and P. E. Lagasse, "Loss calculation and design of arbitrary curved integrated-optic waveguide," J. Opt. Soc. Am. **73,** 177–182 (1983).
10. M. D. Fleit and J. A. Fleck, Jr., "Light propagation in graded-index optical fibers," Appl. Opt. **17,** 3990–3998 (1978).
11. M. D. Feit and J. A. Fleck, Jr., "Computation of mode eigenfunctions in graded-index optical fibers by the propagating beam method," Appl. Opt. **19,** 2240–2246 (1980).
12. A. W. Snyder and R. A. Sammut, "Fundamental (HE_{11}) modes of graded optical fibers," J. Opt. Soc. Am. **69,** 1663–1670 (1979).
13. M. J. Adams, *An Introduction to Optical Waveguides* (Wiley, New York, 1981), p. 132.
14. E. Brinkmeyer, "Spot size of graded-index single-mode fibers: profile-independent representation and new determination method," Appl. Opt. **18,** 932–937 (1979).
15. H. Matsumura and T. Suganuma, "Normalization of single-mode fibers having an arbitrary index profile," Appl. Opt. **19,** 3151–3158 (1980).
16. C. D. Hussey and C. Pask, "Characterizations and design of single-mode optical fibers," Opt. Quantum Electron. **14,** 347–358 (1982).